Annals of Botany **132**: 1159–1174, 2023
https://doi.org/10.1093/aob/mcad107, available online at www.academic.oup.com/aob

ANNALS OF BOTANY
Founded 1887

PART OF A FOCUS ISSUE ON POLLINATION AND FLORAL REGULATION

Unusual nuclear structures in male meiocytes of wild-type rye as revealed by volume microscopy

Sergey Mursalimov[1,2,*], Mami Matsumoto[3,4], Hidetoshi Urakubo[3,5], Elena Deineko[1] and Nobuhiko Ohno[6,7]

[1]Institute of Cytology and Genetics, Siberian Branch of Russian Academy of Sciences, Novosibirsk, 630090, Russia, [2]Institute of Postharvest and Food Sciences, Agricultural Research Organization (ARO)-Volcani Institute, Rishon LeZion, 7505101, Israel, [3]Section of Electron Microscopy, Supportive Center for Brain Research, National Institute for Physiological Sciences, Okazaki, 444-8585, Japan, [4]Department of Developmental and Regenerative Neurobiology, Institute of Brain Science, Nagoya City University Graduate School of Medical Sciences, Nagoya, 467-8601, Japan, [5]Department of Biomedical Data Science, School of Medicine, Fujita Health University, Toyoake, 470-1192, Japan, [6]Department of Anatomy, Division of Histology and Cell Biology, School of Medicine, Jichi Medical University, Shimotsuke, 329-0431, Japan and [7]Division of Ultrastructural Research, National Institute for Physiological Sciences, Okazaki, 444-8585, Japan
[*]For correspondence. E-mail mursalimovsr@gmail.com

Received: 17 May 2023 Returned for revision: 14 July 2023 Editorial decision: 21 July 2023 Accepted: 24 July 2023

• **Background and Aims** During the analysis of plant male meiocytes coming from destroyed meiocyte columns (united multicellular structures formed by male meiocytes in each anther locule), a considerable amount of information becomes unavailable. Therefore, in this study intact meiocyte columns were studied by volume microscopy in wild-type rye for the most relevant presentation of 3-D structure of rye meiocytes throughout meiosis.
• **Methods** We used two types of volume light microscopy: confocal laser scanning microscopy and non-confocal bright-field scanning microscopy combined with alcohol and aldehyde fixation, as well as serial block-face scanning electron microscopy.
• **Key Results** Unusual structures, called nuclear protuberances, were detected. At certain meiotic stages, nuclei formed protuberances that crossed the cell wall through intercellular channels and extended into the cytoplasm of neighbouring cells, while all other aspects of cell structure appeared to be normal. This phenomenon of intercellular nuclear migration (INM) was detected in most meiocytes at leptotene/zygotene. No cases of micronucleus formation or appearance of binucleated meiocytes were noticed. There were instances of direct contact between two nuclei during INM. No influence of fixation or of mechanical impact on the induction of INM was detected.
• **Conclusions** Intercellular nuclear migration in rye may be a programmed process (a normal part of rye male meiosis) or a tricky artefact that cannot be avoided in any way no matter which approach to meiocyte imaging is used. In both cases, INM seems to be an obligatory phenomenon that has previously been hidden by limitations of common microscopic techniques and by 2-D perception of plant male meiocytes. Intercellular nuclear migration cannot be ignored in any studies involving manipulations of rye anthers.

Key words: Meiocyte column, male meiosis, 3-D imaging, volume electron microscopy, cytomixis, intercellular channel.

INTRODUCTION

It is hard to overestimate the importance of meiosis in the life cycle of plants and many other organisms. As a specialized type of cell division producing haploid gametes and ensuring genetic variation, meiosis plays a crucial role in reproduction, and in the case of plants it is directly related to food security issues. Understanding the mechanisms underlying meiosis can provide insights into plant development and may have important applications in plant breeding and crop improvement. Meiosis studies in plants face substantial technical obstacles owing to the inaccessibility of intact meiocytes for direct analysis because they are hidden inside anthers/ovaries surrounded by layers of nourishing and protective cells. Moreover, female meiocytes are available for analysis only in small numbers. Male meiocytes in turn are available for analysis in relatively large numbers and can be extracted as individual cells rather easily. Nonetheless, an even greater obstacle lies beneath the surface in this case. Commonly, male meiocytes are observed on squashed preparations (obtained from a disrupted anther) as individual cells or groups of cells flattened on a slide (Kaur and Singhal, 2019; Ahn *et al.*, 2020). In such a case, even if organelle structure is perfectly preserved, meiocytes lose their intercellular contacts and their 3-D structure is altered. Meanwhile, plant male meiocytes inside each locule of a developing anther exist not as individual cells but as a united multicellular structure referred to as a meiocyte column, meiotic cell column (Li *et al.*, 2012), sporogenous archesporial column (Shunmugam *et al.*, 2018) or meiotic filament (Stronghill *et al.*, 2014). Such a meiocyte column is partially isolated from other tissues, and all meiocytes in it are connected with each other via big

cytoplasmic channels. These special intercellular channels, referred to as cytomictic channels (CCs), are involved in active intercellular transport of essential substances and signalling molecules critical for synchronous meiotic division. Cytomictic channels are considerably larger than plasmodesmata, and even organelles can pass through them (Kumar *et al.*, 2013; Munro *et al.*, 2014; Li and Xu, 2019; Dukowic-Schulze and van der Linde, 2021; Somashekar *et al.*, 2023). Most CCs are disrupted in squashed preparations.

Thus, during an analysis of meiocytes coming from destroyed columns, as seems to be the case for most common microscopic protocols (Kaur and Singhal, 2019; Ahn *et al.*, 2020), a considerable amount of information becomes unavailable, e.g. data about their intact structure, 3-D position inside an anther locule and the functioning of their CCs. Sections obtained from anthers embedded in any type of resin provide only 2-D data (Kolczyk *et al.*, 2015; Bennici *et al.*, 2019; Fadón *et al.*, 2019), and all the information outside a section plane is lost. We regard volume microscopy combined with protocols that allow preservation of the intact 3-D structure of meiocyte columns as the best way to overcome the aforementioned technical problems. Both volume light microscopy (vLM) and volume electron microscopy (vEM) could be used for this purpose.

The most impressive results are likely to be obtained by vEM techniques, such as serial block-face scanning electron microscopy (SBF-SEM), and enable a 3-D ultrastructural analysis of relatively big volumes of plant tissues containing dozens and even hundreds of cells. This approach combines structure preservation of resin-embedded samples and imaging at ultrastructural resolution (Harwood *et al.*, 2020; Ono *et al.*, 2022). Until now, only a single attempt to analyse the interior of intact plant meiocytes has been made by vEM; tobacco meiocyte columns were fixed and embedded in a resin as a part of whole anthers and analysed by SBF-SEM at different stages of meiosis (Mursalimov *et al.*, 2021). The most striking observation in that work was the detection of unusual structures – nuclear protuberances (NPs) – formed by nuclei of most tobacco meiocytes at the first meiotic prophase. These NPs cross the cell wall through the CCs and extend into the cytoplasm of a neighbouring cell, while all other aspects of cell structure appear to be normal (Mursalimov *et al.*, 2021).

Such a phenomenon of intercellular nuclear migration (INM) is not something new or unique for plant male meiosis. It was discovered more than a century ago (Arnoldy, 1900; Koernicke, 1901; Gates, 1908, 1911; Heslop-Harrison, 1966; Feijo and Pais, 1989) and described many times in male meiosis of different plant species, including tobacco (He *et al.*, 2004; Pécrix *et al.*, 2011; Liao *et al.*, 2020; Reis *et al.*, 2022). As a rule, it is referred to as cytomixis but can also be called chromatin body extrusions (Giorgetti *et al.*, 2007) or nuclear envelope protrusions (Sheehan and Pawlowski, 2009; Varas *et al.*, 2015). The causes, mechanisms and consequences of INM are still unclear (for review see Mursalimov and Deineko, 2018). It is generally accepted that INM results in the formation of micronuclei (Barton *et al.*, 2014; Reis *et al.*, 2016). Nonetheless, some researchers consider INM a process that gives rise to binucleated meiocytes, which can subsequently result in the production of unreduced pollen (Farooq *et al.*, 2014; Fakhri *et al.*, 2016; Djafri-Bouallag *et al.*, 2019; Tel-Zur *et al.*, 2020). Direct fusion events, where an NP crosses the cell wall and fuses with a nucleus of a neighbouring cell via a nuclear bridge with unknown consequences, have also been documented (Mursalimov and Deineko, 2011). Some investigators view INM as a response to stress (Kalinka *et al.*, 2010; Kravets, 2011; Kravets *et al.*, 2022). Nevertheless, most of these scientists have regarded INM as a rare deviation. The results obtained by SBF-SEM on tobacco allow a preliminary conclusion that INM is a constant part of normal male meiosis, at least in tobacco. If so, it seems that INM has been greatly underestimated so far owing to limitations of conventional microscopic protocols. It is possible that such underestimation could have happened in hundreds of other plant species where INM has been documented (He *et al.*, 2004; Pécrix *et al.*, 2011; Mursalimov *et al.*, 2013; Páez *et al.*, 2021). It appears that fast-developing volume microscopy techniques may allow us for the first time in a century to discern the real picture of INM in plant meiosis, thereby enabling researchers to determine its causes and consequences and perhaps even ways to manipulate it.

Besides serial sectioning and imaging of resin-embedded samples by such techniques as SBF-SEM, the 3-D structure of intact meiocyte columns can be studied by vLM techniques. For this purpose, it is desirable to use plant species with relatively big meiocyte columns that can be easily dissected from anthers. The direct examination of meiocyte columns helps to increase resolution sufficiently and provides a sharper image of the cells. Preservation of the intact structure of meiocyte columns is critical in this context. We did not find articles where meiocyte columns were dissected with preservation of their intact 3-D structure and imaged by vLM at magnification/resolution sufficient for NP detection.

Thus, the application of volume microscopy to the analysis of intact meiocyte columns can greatly expand our understanding of meiosis features in various plant species. Aside from INM, it remains to be determined how many other cellular structures and mechanisms underlying meiosis remain undiscovered owing to 2-D perception of meiocyte structure.

Here we employed a combination of four protocols including cryofixation and alcohol and aldehyde fixation and both vLM and vEM for the most relevant presentation of 3-D structure of rye meiocytes throughout meiosis with special attention to the detection of INM cases. We found that most rye male meiocytes participate in INM at the first meiotic prophase. The proposed approach can be used in the same manner for investigation of meiocyte columns of other cereals, e.g. wheat or barley, and with some modifications in many other plant species. In addition to INM research, this approach may be used for a variety of meiosis studies requiring preservation of the 3-D structure of male meiocytes.

MATERIALS AND METHODS

Plant material

Wild-type rye plants (*Secale cereale* L. cv. 'Onokhoiskaya', $2n = 14$, RR) from the collection at the Institute of Cytology and Genetics (Novosibirsk, Russia) were grown in a greenhouse with a photoperiod of 16/8 h (day/night) at a temperature of 22/18 °C (day/night). Two independent series of growing

and sampling of the plants were performed in May–June and September–October of 2021. The material was collected between 0900 and 1200 h local time. The emergence of the flag leaf was utilized for estimation of meiotic stages of interest. No touching by fingers or other mechanical impacts were applied to developing spikes.

Cryofixation followed by routine bright-field microscopy

For cryofixation [presented as (i) in Fig. 1A], spikes were dissected from plants within leaf sheaths to avoid mechanical impact on meiocytes. The first incision was made beneath a spike, and the whole upper part of a plant was detached from the roots and fully plunged into liquid nitrogen. After that, the second incision was made above the spike within leaf sheaths without a single touching a plant fragment containing the spike (i.e. there was no mechanical influence on the spike). Then, 50-mL tubes containing the cryofixed material were transferred to an ultra-low-temperature (−70 °C) freezer, where, after full nitrogen evaporation, they were filled with acetic alcohol (absolute ethanol/glacial acetic acid at 3:1) precooled to −70 °C and left at this temperature for a week for cryosubstitution. Next, the tubes were incubated at −20 °C for 12 h; then, the fixative was replaced by fresh fixative precooled to −20 °C. After 24 h, the samples were incubated at 4 °C for 5 h. Then, the fixative was replaced again with fresh fixative precooled to 4 °C. After overnight incubation, the material was kept at room temperature and the fixative was replaced with 70 % ethanol for storage. Before analysis, the spikes were dissected from leaf sheaths, and then anthers were dissected from spikes and squashed on a slide with a dissection needle and stained with a drop of 6 % acetocarmine. The stained meiocytes were examined by conventional bright-field microscopy under an Axio Observer Z1 microscope equipped with an AxioCam HRc camera (Zeiss, Germany). The experiment was conducted two times independently. In each repetition, material was obtained from three independent plants, and at least 100 meiocytes from every plant were analysed.

Meiocyte column extraction

Male meiocyte columns were analysed after alcohol and aldehyde fixation. The corresponding procedures of processing of the material are presented in the scheme in Fig. 1A as (ii) and (iii). For alcohol fixation (ii), spikes were dissected from plants within leaf sheaths to avoid mechanical impact on meiocytes and were immersed in absolute methanol, acetic alcohol (absolute ethanol/glacial acetic acid at 3:1) or Carnoy's solution (absolute ethanol/chloroform/glacial acetic at 6:3:1). Both ice-cold and room temperatures were used for every mentioned fixative. In every case, the fixative was replaced with a fresh one after 30 min and then replaced one more time after 1 h and left overnight. On the next day, the fixative was gradually replaced by 1 × phosphate-buffered saline (PBS, pH 7.2). The material was transferred into 70, 50 and 30 % ethanol solutions and then 1 × PBS (pH 7.2), with incubation for 1 h in each. After that, the spikes were dissected from the leaf sheaths and post-fixed in 8 % formaldehyde (Sigma–Aldrich, USA) in 1 × PBS overnight. The formaldehyde treatment is critical for successful extraction of meiocyte columns. After overnight incubation, the material was washed three times in 1 × PBS for 1 h. Before analysis, anthers were dissected from spikes and cut into two pieces with syringe needles, after which, by applying gentle pressure by means of a dissection needle, we extracted meiocyte columns from the anther fragments. The experiment was conducted two times independently for every type of alcohol fixative. Three to five plants were used in each repetition. At least three meiocyte columns from every plant were analysed.

For aldehyde fixation (iii), spikes were carefully dissected from the plants before fixation to ensure better accessibility of meiocytes to a fixative. The dissected spikes were immersed in 8 % formaldehyde (Sigma–Aldrich, USA) in 1 × PBS for at least 48 h of incubation either on ice or at room temperature. Then, the material was washed three times with 1 × PBS for 1 h. Before analysis, anthers were dissected from spikes, and meiocyte columns were extracted as described above. The samples were obtained from 50 individual rye plants, and 115 meiocyte columns prepared this way were investigated (Table 1).

Volume light microscopy

Two types of vLM were employed for meiocyte column imaging: confocal laser scanning microscopy (CLSM) and non-confocal bright-field scanning microscopy (BFSM) (Senft *et al.*, 1990).

Confocal laser scanning microscopy

A drop of SYTOX Green (Invitrogen, USA) at 1 μM in 1 × PBS was placed on a slide with the dissected meiocyte columns for fluorescent staining of nuclei. Then, the slide was transferred to a moisture chamber for 30 min of incubation at room temperature. Then, meiocyte columns were mounted on ProLong Diamond antifade medium (Invitrogen, USA) and analysed using an LSM 780 device (Zeiss, Germany). Green fluorescence was excited with a 488-nm laser. The images were captured and processed by Zen software (Zeiss, Germany).

Non-confocal bright-field scanning microscopy

A drop of 6 % acetocarmine was placed on a slide with the dissected meiocyte columns for routine tissue staining. Without washing or adding a mounting medium, the columns were immediately coverslipped and nail polish was applied around the coverslip edges to prevent drying of the sample. Serial optical sections of the stained meiocyte columns were acquired by means of an Axio Observer Z1 bright-field microscope equipped with an AxioCam HRc camera (Zeiss, Germany). A Z-stack containing 10–30 serial images with a step of 1 μm was obtained for every selected region. Zen software was used for image capturing and initial analysis. Next, the image stacks were imported into Dragonfly software (ORS, Canada) for subsequent analysis, segmentation and 3-D modelling.

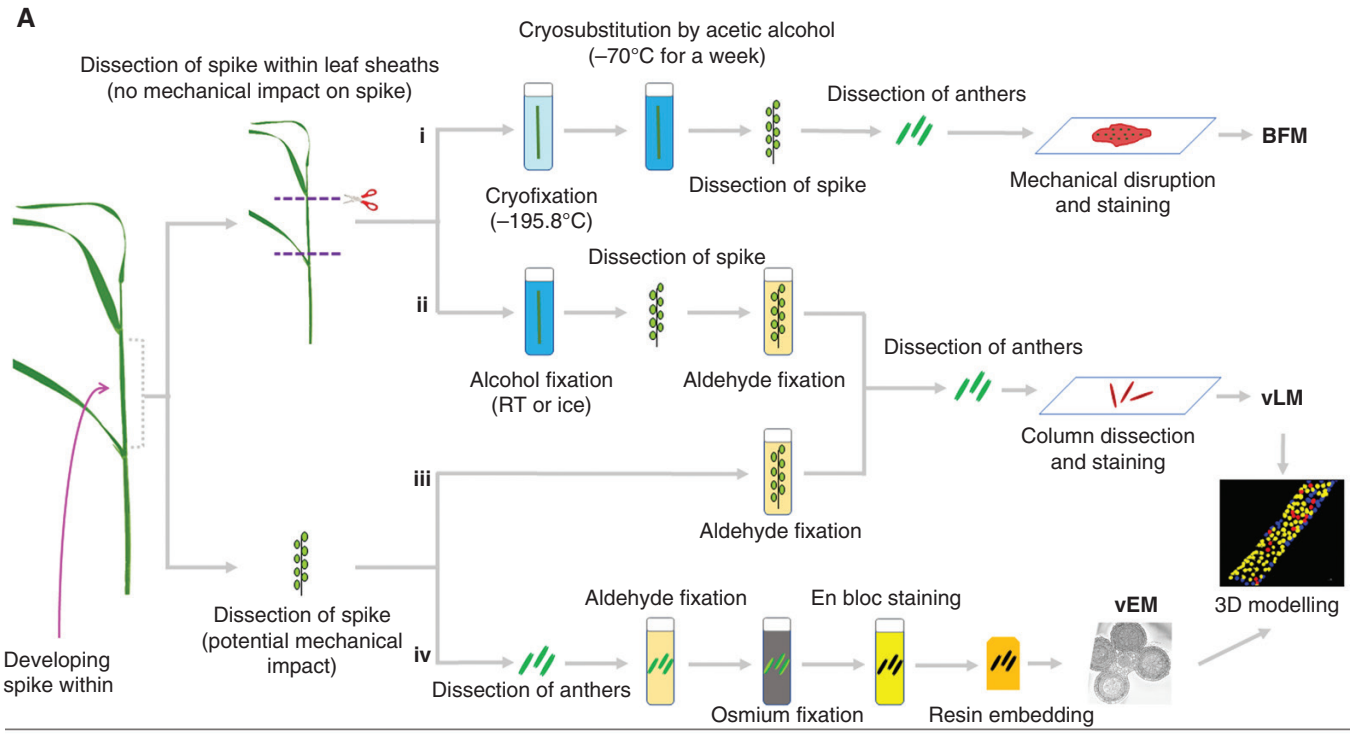

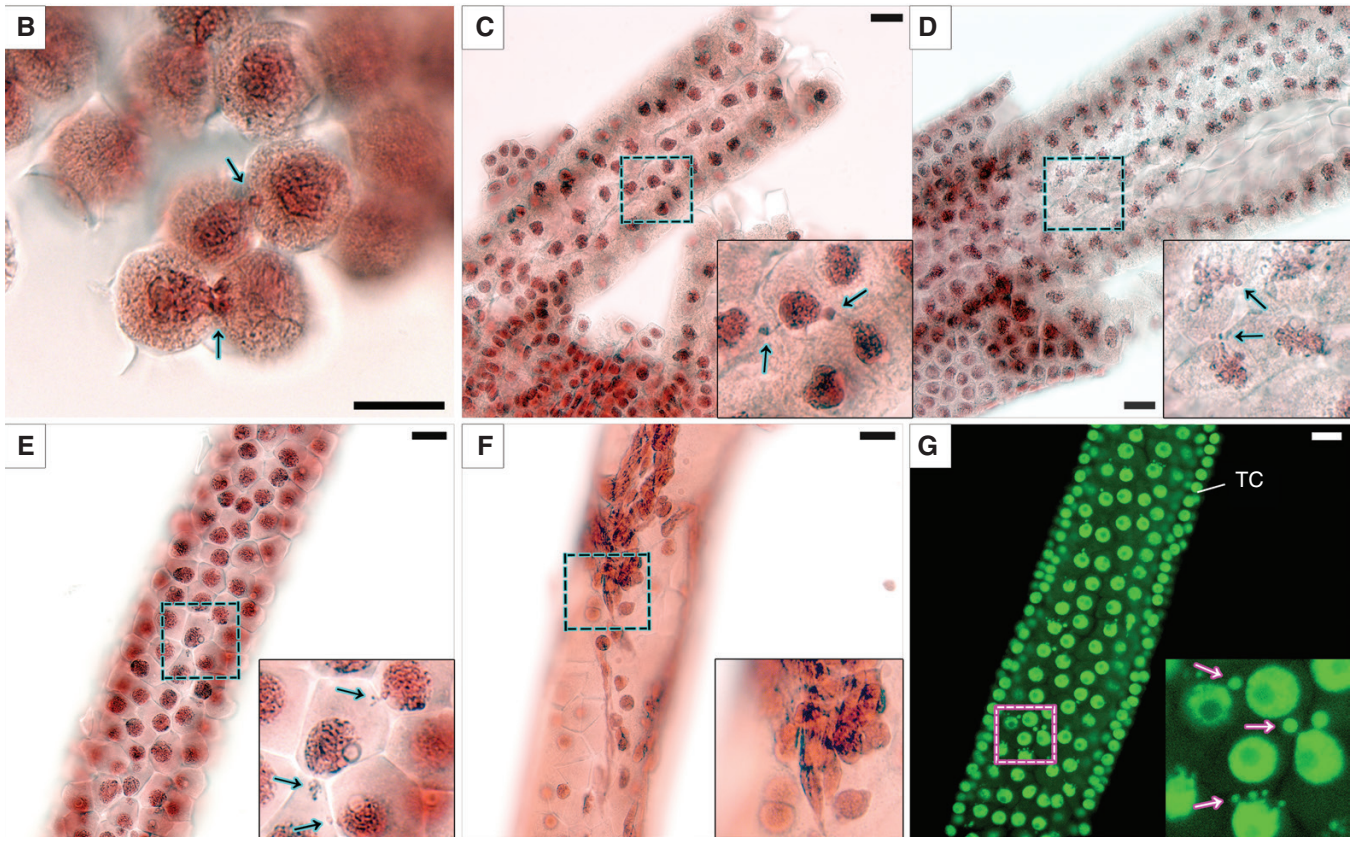

FIG. 1. Protocols of sample preparation used in this work (i–iv) and resulting images of rye meiocyte columns, as obtained by vLM at early meiotic prophase I. (A) Outline of the experiment. RT, room temperature. (B) Meiocytes after cryofixation were analysed by light microscopy (Ai). (C, D) Meiocyte columns after alcohol fixation were examined by light microscopy (Aii). Column fixed in ice-cold methanol (C) and fixed in acetic alcohol (D). (E–G) Meiocyte columns after aldehyde fixation as examined by light microscopy (Aiii). (E, G) Well-preserved meiocyte columns. (F) Column with damaged meiocytes. Acetocarmine staining and bright-field microscopy (BFM) are shown in (B–F). SYTOX Green staining and confocal laser scanning microscopy (maximum intensity projection) are presented in (G). Arrows point to NPs crossing a cell wall. Boxed regions are magnified in inserts. TC, tapetal cells. Scale bars = 20 μm.

TABLE 1. *INM frequencies in meiocyte columns as determined by BFSM at different meiotic stages.*

Meiotic stage	Number of meiocyte columns	Observed cells	Cells not involved in INM		Cells involved in INM	
			number	%	Number	%, mean ± s.d.
Premeiosis	18	2202	2202	100	0	0
Leptotene/zygotene	44	4687	1150	5.84	3537	76.93 ± 11.93
Pachytene	23	1326	1322	99.76	4	0.24 ± 0.88
Diplotene/diakinesis	17	1024	1018	99.71	6	0.29 ± 1.23
Metaphase I	13	568	568	100	0	0

Volume electron microscopy

We used SBF-SEM to study the ultrastructure of meiocyte columns. Aldehyde fixation (iv) was used to prepare meiocyte columns for SBF-SEM. Spikes were carefully dissected from plants before fixation, and then anthers were dissected with extra care from the spikes on an ice-cold plate. Then, the anthers were fixed with 2.5 % paraformaldehyde and 2.5 % glutaraldehyde in 1 × PBS overnight on ice. The following steps of preparation, imaging and analysis of SBF-SEM samples have been described previously for tobacco anthers (Mursalimov *et al.*, 2021). Briefly, after aldehyde fixation, the anthers were cut into 200- to 300-µm pieces. Then, the tissue samples were treated with reduced osmium tetroxide, thiocarbohydrazide and osmium tetroxide again. After *en bloc* staining with uranyl acetate and lead aspartate, the tissue samples were dehydrated and embedded in epoxy resin. After examination of semithin sections for selection of regions of interest, mounting on aluminium rivets, trimming and gold evaporation for increasing surface conductivity, the blocks were imaged under a field emission scanning electron microscope (Merlin or Sigma, Zeiss, Germany) equipped with 3View (Gatan, USA). The following scanning parameters were applied to the samples presented in SBF-SEM figures. We obtained 1419 individual images of the premeiotic stage (accelerating voltage, dwelling time, pixel size in *X* and *Y* directions and slicing thickness in the *Z* direction; pixel dimensions of each image were 1.3 kV, 0.9 µs, 6.93 nm, 50 nm and 12288 × 12288 pixels, respectively, without tiling); 1590 images of the leptotene stage (1.3 kV, 1.0 µs, 6 nm, 50 nm and 9216 × 9216 pixels with 2 × 2 tiling); 1839 images of the zygotene stage (1.3 kV, 1.0 µs, 6 nm, 50 nm and 13312 × 13312 pixels with no tiling); and 1291 images of the pachytene stage (1.2 kV, 0.9 µs, 7 nm, 70 nm and 10240 × 10240 pixels with 2 × 2 tiling). After binning, stitching and alignment on Fiji (Schindelin *et al.*, 2012), a training dataset for nuclei and cell walls was produced with Dragonfly software (ORS, Canada), Microscopy Image Browser (Belevich *et al.*, 2016) and Amira 6.2.0 software (FEI Visualization Science Group, USA). Semi-automatic segmentation with cycles of training, inference and proofreading was performed with the help of a 2-D-convoluted neural network in a unified environment for CNN-based automated segmentation of electron microscopy images (UNI-EM) (Urakubo *et al.*, 2019). The acquired prediction maps were manually proofread, and 3-D reconstruction was performed in Amira 6.2.0. In total, eight fragments of meiocyte columns at different meiotic stages were obtained from independent plants and subjected to analysis (Table 2).

RESULTS

Four approaches complementing one another were used for the fixation and imaging of developing rye male meiocytes (Fig. 1A). Cryofixation [Fig. 1A (i)] and alcohol fixation [Fig. 1A (ii)] combined with light microscopy were utilized to demonstrate that INM is not induced by chemical or mechanical impact. Aldehyde fixation combined with light [Fig. 1A (iii)] and electron microscopy [Fig. 1A (iv)] was used to analyse the frequency of INM and fine cell structure of meiocytes, respectively.

For cryofixation (i), whole spikes within leaf sheaths were plunged into liquid nitrogen followed by cryosubstitution. The meiocyte columns cannot be dissected from rye anthers after such a treatment, and squashed preparations were made to observe cryofixed meiocytes. The meiocytes examined by conventional bright-field microscopy were represented by groups of cells on these preparations (Fig. 1B). They had dense cytoplasm and nuclei, which were found to be intensely stained by acetocarmine. The structure of chromosomes within these dense nuclei was barely visible, but disrupted nuclei or structureless chromatin was not observed. Multiple cases of typical INM were detected in cryofixed meiocytes at early prophase I.

For the alcohol fixation (ii), whole spikes within leaf sheaths were immersed in methanol, acetic alcohol or Carnoy's solution. After such processing, meiocyte columns could be dissected as united structures from rye anthers (Fig. 1C, D, Supplementary Data Fig. S1). Cells in the resulting meiocyte columns had rather dense nuclei and cytoplasm; however, the structure of chromosomes was more clear-cut than in cryosubstituted meiocytes. Intercellular nuclear migration was constantly present in the meiocyte columns at early prophase I regardless of the type of alcohol fixative that was used: methanol (Fig. 1C), acetic alcohol (Fig. 1D) or Carnoy's solution (Supplementary Data Fig. S1). No disrupted nuclei or structureless chromatin were found.

In the case of aldehyde fixation, whole spikes within leaf sheaths cannot be properly fixed owing to the rather weak penetration ability of aldehyde fixatives. This situation required dissection of spikes (iii) or anthers (vi) before fixation to obtain well-preserved cells. We used two types of aldehyde fixative: formaldehyde (iii) for the light microscopic examination and a mixture of paraformaldehyde and glutaraldehyde (vi) for SBF-SEM. Before formaldehyde fixation, the spikes were dissected from the plants and immersed in the fixative (iii). After such fixation, the meiocyte columns could be dissected from anthers easily. In most cases, the meiocyte columns obtained

Table 2. *INM frequencies in meiocyte columns as determined by SBF-SEM at different meiotic stages.*

Meiotic stage	Sample (anther fragment)	Examined cells	Cells not involved in INM		Cells involved in INM	
			Number	%	Number	%
Premeiosis	1	123	123	100	0	0
	2	67	67	100	0	0
Leptotene	3	94	16	17.02	78	82.98
	4	41	6	14.63	35	85.37
Zygotene	5	64	4	6.25	60	93.75
Pachytene	6	80	80	100	0	0
	7	18	18	100	0	0
	8	17	17	100	0	0

this way had perfect structural preservation of cells with clear transparent cytoplasm and a distinguishable thread-like content of meiocyte nuclei (Fig. 1E, G). Intercellular nuclear migration was constantly present in these meiocyte columns at early prophase I, and they were used for subsequent analyses. In some cases, severely damaged meiocytes with disrupted cell walls and structureless chromatin were noted in the dissected meiocyte columns after formaldehyde fixation (Fig. 1F). Such columns were excluded from further analysis.

The well-preserved meiocyte columns fixed by acetic alcohol and formaldehyde were studied throughout meiosis by vLM. Both routine and fluorescent staining were tested for the visualization of nuclei in the meiocyte columns. Acetocarmine yielded sufficient staining of nuclei for bright-field microscopy (Fig. 1B–F), as did SYTOX Green for fluorescence microscopy (Fig. 1G, Supplementary Data Fig. S1).

The most noticeable changes in their structure were detectable at the first meiotic prophase (Fig. 2). Before entering meiosis, male meiocytes of rye have a triangular shape and a big nucleus with uncondensed chromatin and big nucleoli (Fig. 2A–C). Meiocytes were found to be tightly packed together, and no callose wall was observed. In transverse view, meiocytes looked like sectors of a circle, and there was no space in its central region (Fig. 2A). No cases of INM were detectable at this stage. For this reason, in 3-D models the nuclei available for analysis at this stage were represented only by non-migrating nuclei (Fig. 2C, Supplementary Data Video S1).

After entering meiosis, at leptotene/zygotene, nuclei of meiocytes became more condensed and thread-like structures appeared inside them (Fig. 2D–F). An intense process of callose wall formation could be seen at this stage. It proceeded unevenly; predominantly, callose deposits arose in the part of the meiocytes oriented to the centre of a meiocyte column. The callose had no colour, and its unequal deposition formed a transparent spine in the centre of the meiocyte column; it was noticeable in the transverse view (Fig. 2D, Supplementary Data Video S2). Multiple cases of INM were registered in meiocytes at the leptotene/zygotene stage. The NPs formed by migrating nuclei were either barely visible (Fig. 2E_1, E_2, Supplementary Data Fig. S1) or quite prominent (Fig. 2D_1, E_3). The analysis of the image stacks obtained during the scanning of the meiocyte columns revealed that INM occurs in most meiocytes at leptotene/zygotene. Accordingly, most of the nuclei were represented by migrating ones in 3-D models (Fig. 2F, Supplementary Data Video S3).

During the transition to the pachytene stage, meiocytes changed their shape from triangular to spherical, and their nuclei became even more condensed (Fig. 2G–I). Meiocytes started losing their connections, and a rather big central cavity formed in the meiocyte columns at this stage. This cavity was not filled with callose, which was still observable as colourless structures located on the edge of the cavity (Fig. 2G). With rare exceptions, INM was not detectable in meiocytes at this stage. In the 3-D model of the meiocyte column at pachytene, all the nuclei available for analysis in the chosen sample were designated as non-migrating ones (Fig. 2I, Supplementary Data Video S4). The most noticeable alteration of the structure of meiotic columns at diplotene/diakinesis and metaphase I and at subsequent stages of meiosis was gradual enlargement of the central cavity (Supplementary Data Fig. S1). No INM cases were found in meiocytes starting from metaphase I.

To assess the frequency of INM in rye male meiosis, 115 individual meiocyte columns fixed in formaldehyde were dissected from anthers and investigated by vLM (Table 1). Acetocarmine staining combined with BFSM was performed for this purpose. In total, 9807 meiocytes at different meiotic stages were analysed. Special attention was paid to leptotene/zygotene, where meiocyte columns obtained from 44 anthers were examined. Only meiocyte columns with well-preserved 3-D structure and clearly visible cell walls and nuclei were subjected to this analysis. Not a single case of INM was noted in 18 meiocyte columns (totally containing 2202 meiocytes) at the premeiotic stage (Table 1). INM frequency drastically increased at leptotene/zygotene. In different meiocyte columns, 53.99–100 % of meiocytes were involved in INM as a nuclear donor/recipient or both (76.93 % on average). Meiocyte columns without INM were absent at this stage. Starting from pachytene until diakinesis, INM frequency decreased drastically (to 0.24–0.29 %), and INM was not detectable after metaphase I. No cases of separation of NPs from their nuclei during migration were found. No micronuclei were found in any of the studied cells. No cases of direct fusion between two nuclei or of formation of binucleated meiocytes were detected by vLM.

Although vLM showed relatively high abundance of INM at leptotene/zygotene, vEM via SBF-SEM was necessary to address questions such as the presence or absence of CCs required for INM, unequivocal lack of even small NPs migrating to adjacent cells at certain stages, and physical interactions between migrating nuclei and surrounding organelles. For

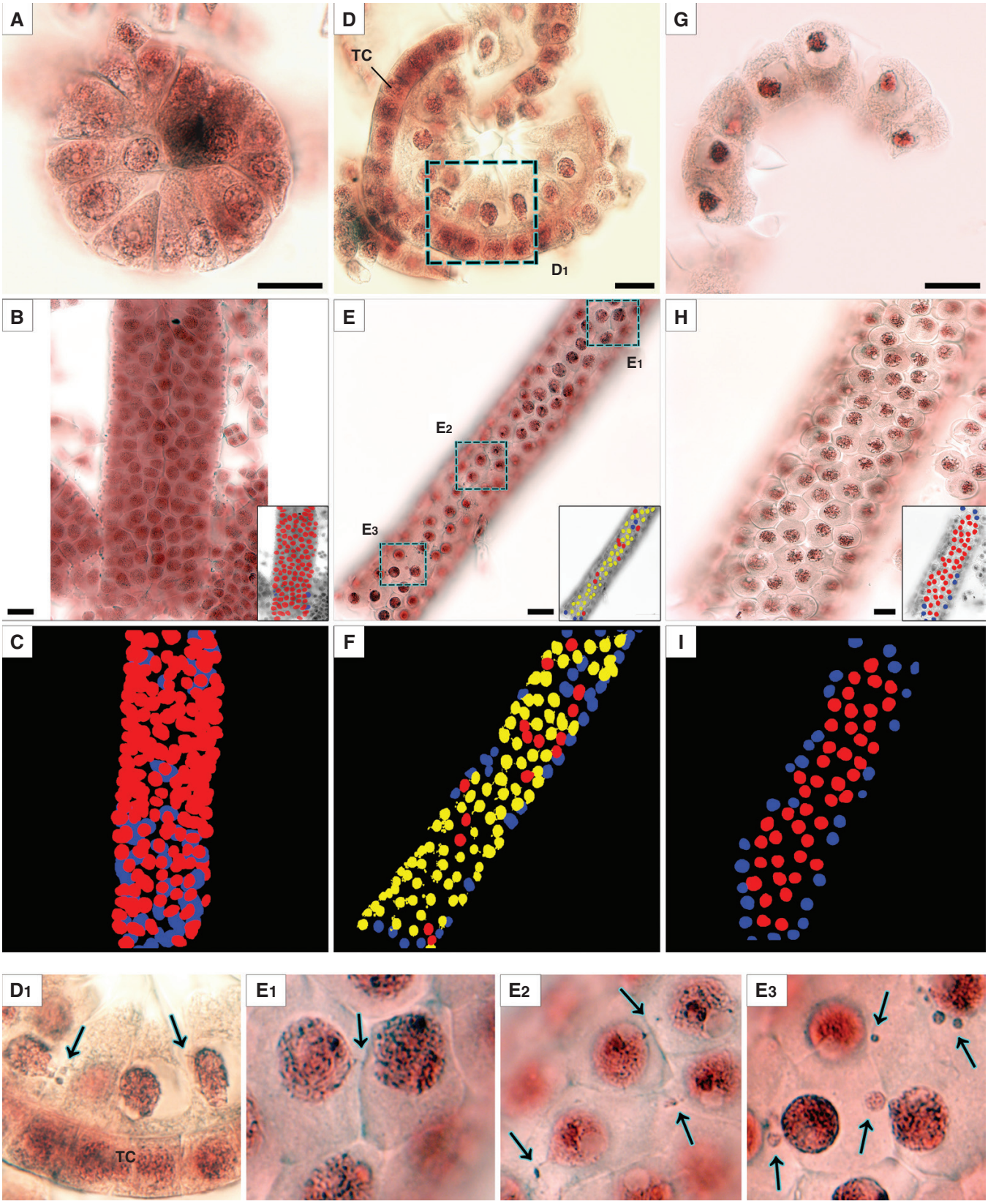

FIG. 2. Meiocyte columns of rye at the premeiotic stage (A–C), leptotene/zygotene (D–F) and pachytene (G–I) according to light microscopy. (A, D, G) Transverse view of meiocyte columns. (B, E, H) Longitudinal view of a column, represented by an individual optical section from an image stack containing 23 images in (B), 18 in (E) and 11 in (H). In the insets, the same individual images are grey-scaled with manually painted nuclei. (C, F, I) 3-D reconstructions of scanned meiocyte columns with painted nuclei. (D_1) and (E_{1-3}) are enlarged fragments. Alcohol fixation in (A, D, G), and formaldehyde fixation in other panels. The yellow colour denotes migrating nuclei, red non-migrating nuclei, and blue partially scanned nuclei (their status is not clear). Arrows point to NPs crossing a cell wall. TC, tapetal cells. Scale bars = 20 μm.

SBF-SEM, rye anthers were dissected from plants before immersion in fixative [Fig. 1A (iv)]. After the osmium treatment, *en bloc* staining and resin embedding, samples containing meiocytes at premeiotic, leptotene, zygotene and pachytene stages were scanned. General structure of the meiocyte columns imaged by SBF-SEM was well consistent with that determined by vLM. Owing to the relatively small size of the fragments of meiocyte columns scanned by SBF-SEM, leptotene and zygotene stages could be separated and analysed individually, in contrast to vLM, where scanned columns often contained meiocytes at both stages.

At the premeiotic stage, meiocytes were represented by triangular tightly packed cells (with a big oval-shaped nucleus containing uncondensed chromatin and multiple complex nucleoli) surrounded by tapetal cells (Fig. 3A–D, Supplementary Data Video S5). SBF-SEM helped to observe structures hidden from vLM, such as CCs connecting meiocytes (Supplementary Data Fig. S2). Despite the presence of fully formed CCs, no cases of INM were found in meiocytes at this stage even at ultrastructural resolution. Accordingly, most of the nuclei were represented by non-migrating ones in the 3-D model (Fig. 3C, D). In total, 190 meiocytes from two independent fragments of meiocyte columns were analysed at this stage (Table 2).

At leptotene, meiocytes were still close to a triangle in shape and tightly packed (Fig. 3E–H, Supplementary Data Video S6). It was noticeable that chromatin became more condensed, the nucleoli started losing their complex structure, and their number decreased; the callose deposits began at the centre of meiocyte columns. The number of CCs connecting meiocytes went up significantly at his stage (Supplementary Data Fig. S2). Most of the meiocytes participated in INM at leptotene, and their nuclei were designated as migrating ones in a 3-D model (Fig. 3G, H). In total, 135 meiocytes in two fragments of independent meiocyte columns were examined at this stage, and 113 of them (~84 %) were involved in INM (Table 2).

At the zygotene stage, the meiocytes gradually lost their triangular shape, chromatin became even more condensed, and as a rule only one nucleolus could be observed in meiocyte nuclei. The callose deposition formed a prominent transparent spine in the centre of the meiocyte columns at this stage (Fig. 3I–L, Supplementary Data Video S7). Although some CCs were closed by the callose deposits, there were still hundreds of them open and connecting meiocytes at this stage (Supplementary Data Fig. S2). Sixty-four meiocytes in one randomly chosen meiocyte column were investigated at this stage, and 60 of them (about 94 %) took part in INM (Table 2). The 3-D model of a meiocyte column fragment at zygotene revealed predominance of migrating nuclei (highlighted in yellow in Fig. 3K, L). It should be noted that even if a nucleus did not migrate and was highlighted in red in the 3-D model, the cell could still be involved in INM as a recipient of a nucleus migrating from a neighbouring meiocyte.

At pachytene, the shape of meiocytes tended to become more spherical, and cells in meiocyte columns were located around a rather big central cavity (Fig. 3M–P, Supplementary Data Video S8). This central cavity consisted of intercellular space with no structural content except for remains of the callose wall. Meiocytes located in this cavity that were separated from all the others were seen occasionally. They did not differ significantly in their structure from the other meiocytes and looked viable (Fig. 3N, O). It was also noticeable that the cytoplasm of the tapetal cells surrounding meiocytes became dense, and they stained more intensively at this stage. In total, 115 meiocytes from three independent fragments of meiocyte columns were analysed at this stage (Table 2). No cases of INM was found, although most meiocytes were still connected by dozens of CCs (Supplementary Data Fig. S2). Accordingly, the scanned nuclei were represented by non-migrating ones in the 3-D model (Fig. 3O, P). No cases of CC formation between meiocytes and tapetal cells were noted at any stage. It should be pointed out that a few damaged meiocytes and tapetal cells with disrupted cell walls and structureless chromatin were observed in almost every meiocyte column at every studied meiotic stage; chromatin in the damaged meiocytes is highlighted in orange in the 3-D models.

SBF-SEM uncovered some NP formation patterns that cannot be detected by other microscopic techniques (Fig. 4). It was shown that, despite the absence of INM at the premeiotic stage, the nuclei of meiocytes form NPs at this moment, and these NPs are often headed to the cell wall but do not cross it owing to their limited length (Fig. 4A–D). At leptotene, the size of NPs was greatly variable. There were NPs 1 μm in length, which were rather tiny compared with nucleus size (Fig. 4E–H), as well as extended NPs having length almost the same as a nucleus diameter: ~15 μm (Fig. 4I–L). Nucleus–nucleus contacts between the migrating nuclei and the nuclei of neighbouring meiocytes were observed at zygotene (Fig. 4M–P). In such cases, the gap between the nuclear membranes of the migrating NP and the nucleus of a neighbouring meiocyte became undistinguishable on certain sections. At the zygotene stage, along with the NPs crossing the cell wall, NPs that did not cross the cell wall, just as at the premeiotic stage, were registered (Fig. 4Q–T). In all the above-mentioned cases, nuclei forming the NPs maintained the central position in their own cell, the nuclei had a rather spherical shape, and their nuclear envelopes showed no signs of damage. We did not detect any NPs by SBF-SEM at pachytene.

It was confirmed by 3-D ultrastructural analysis that in rye meiosis NPs never detached from the nucleus from which they originated. No cases of micronucleus formation or formation of binucleated meiocytes were found in the cells evaluated by SBF-SEM at any stage. No cases of INM between meiocytes and tapetal cells were noticed in any studied samples either.

DISCUSSION

There is no perfect technique for investigating plant male meiocytes. Every currently available approach to the analysis of plant male meiocytes allows observation of their intact 3-D structure, fine cellular details and a large number of cells or their living dynamics, but not all together. Such a comprehensive analysis requires a combination of different techniques to study such structures as NPs, which can be easily destroyed or hidden from observation when conventional microscopic techniques are used. For this reason, we utilized four approaches to examine INM in developing rye male meiocytes. Cryofixation and alcohol fixation procedures in the absence of mechanical impact were carried out to characterize overall structure

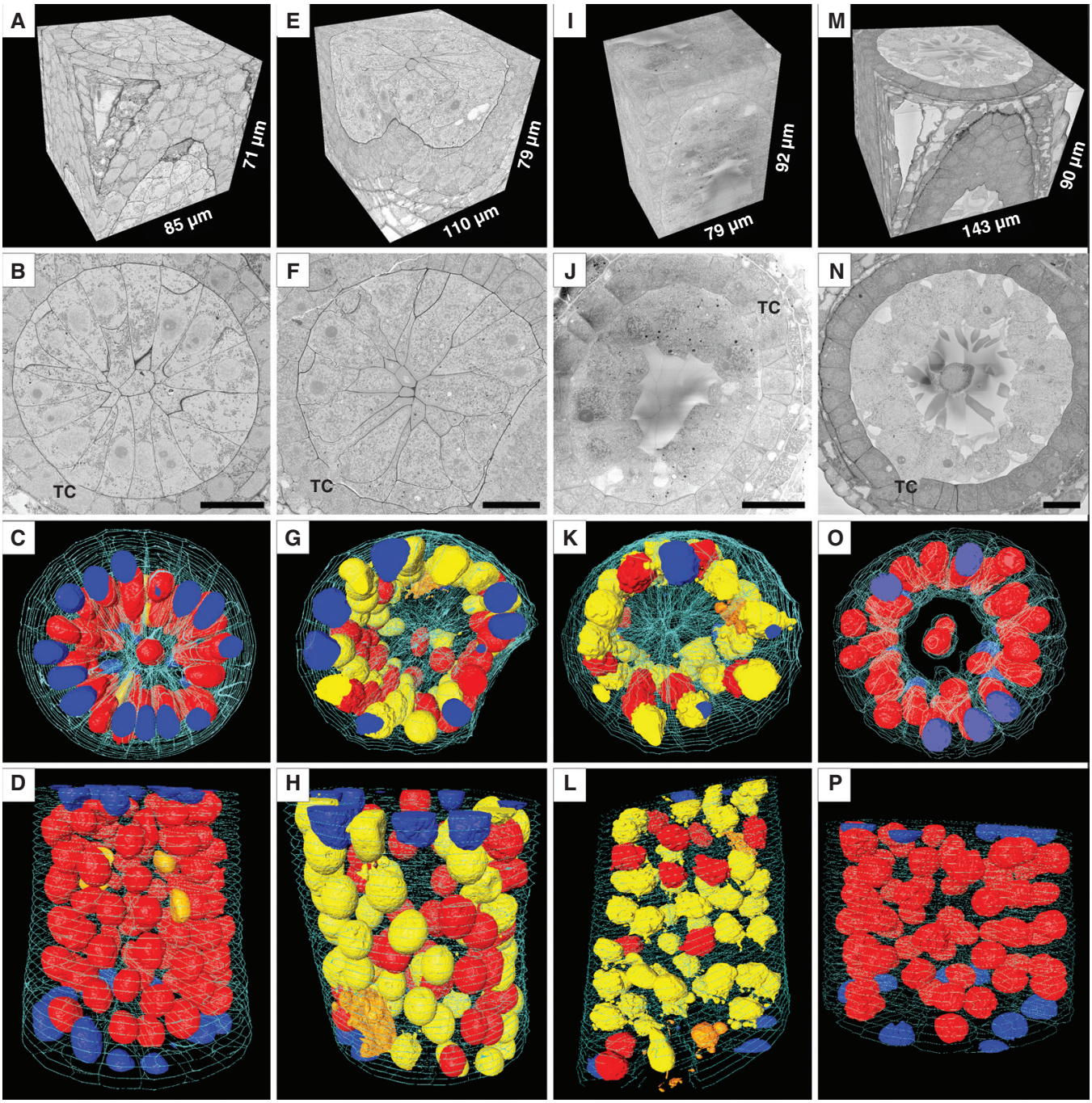

FIG. 3. Fragments of meiocyte columns at the premeiotic stage (A–D), leptotene (E–H), zygotene (I–L) and pachytene (M–P) as examined by SBF-SEM. 3-D reconstructions of scanned tissue fragments from 1429 serial images in (A), 1590 in (E), 1839 in (I) and 1291 in (M). An individual ultrastructural image from a corresponding stack is shown in (B), (F), (J) and (N). 3-D reconstructions of scanned tissue fragments with nuclei and cell walls highlighted by various colours: a transverse view in (C, G, K, O) and a longitudinal view in (D, H, L, P). Yellow denotes migrating nuclei, red non-migrating nuclei, blue partially scanned nuclei (their status is not clear), orange damaged nuclei, and turquoise the outer layer of cell walls, labelled on every 50th slice. TC, tapetal cells. Scale bars = 20 µm.

of intact meiocytes and meiocyte columns by light microscopy. Aldehyde fixation with potential mechanical impact on meiocytes was used for examination of fine cellular structure by light and electron microscopy.

Cryofixation enables a researcher to stop any processes in a fixed tissue at one moment by freezing all fluid phases solid with ice formation. As a rule, quick freezing or high-pressure freezing is chosen to prevent the formation of ice crystals and ensures good membrane preservation for ultrastructural analysis (Ohno *et al.*, 2008; Studer *et al.*, 2008). On the other hand, this approach is suitable for rather small tissue fragments, not bigger than a few micrometres in thickness. In the current work, we opted for plunge-freezing of whole rye spikes within leaf sheaths to obtain meiocytes that are fixed

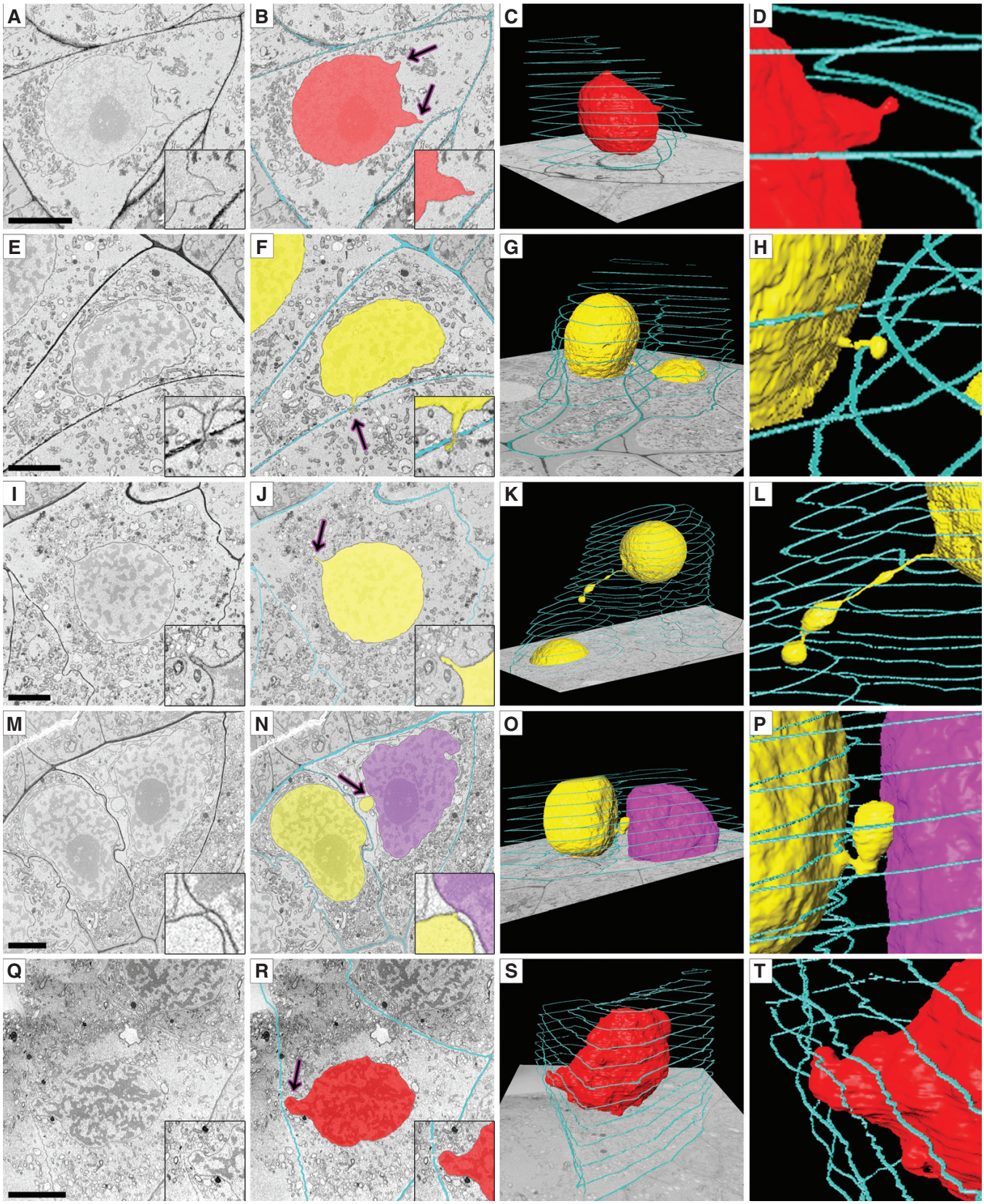

FIG. 4. Dynamics of NP formation in meiocytes imaged by SBF-SEM. Nuclear protuberances emerge but do not cross the cell wall at the premeiotic stage (A–D). At leptotene can be seen tiny NPs (E–H), extended NPs comparable in length to the size of a nucleus (I–L) and NPs forming nucleus–nucleus contacts (M–P). At zygotene NPs that do not penetrate the cell wall appear again (Q–T). The left column presents original images, and to the right the same image is shown with cell walls and nuclei highlighted in various colours, and the two right-hand columns are 3-D reconstructions of the scanned cells and NPs with enlargement. Arrows denote NPs. Yellow and purple indicate nuclei involved in INM, red non-involved nuclei, and turquoise the outer layer of cell walls, labelled on every 25th slice. Scale bars = 5 μm.

without any mechanical or chemical impact. Our samples were sufficiently bigger than needed for cryoelectron microscopy, and plunge-freezing makes ice crystal formation unavoidable in this context. Furthermore, the protein denaturation induced by acetic alcohol during cryosubstitution makes cryofixed meiocytes unsuitable for the analysis of fine cellular structure. Nevertheless, meiocyte structure preservation after such a treatment is acceptable for routine staining and light microscopic observation (Baskin *et al*., 1996; Rensing *et al*., 2002; Ohno *et al*., 2010). This approach helped us to conclude that INM is not induced by mechanical or chemical impact in rye meiocytes.

Previously, we used the same approach to prove the natural presence of INM in tobacco male meiocytes (Mursalimov *et al*., 2022*a*); whole tobacco inflorescences, dissected flower buds and individual anthers were cryofixed in liquid nitrogen by plunge freezing. In that paper, INM was documented in all the studied samples, consistently with the data presented in the current work. Unfortunately, no studies on cryofixation of male meiocytes in other plant species have been conducted to date.

The rapid fixation and high penetration ability of alcohol fixatives allowed us to apply them for the fixation of whole rye spikes within leaf sheaths as well. The resulting meiocyte columns were not affected by any mechanical impact prior to fixation and could be dissected from anthers as a united structure. Moreover, acetic alcohol, which we used the most among alcohol fixatives, makes meiocyte columns quite dense and firm. It allowed us to fragment some meiocyte columns into slices a few cells wide and to see their transverse view as presented in Fig. 2. Our main finding after the testing of different kinds of alcohol fixatives is that fixatives do not influence INM, and INM could be investigated in the absence of any mechanical impact.

Another possible approach to proving that INM is a natural phenomenon is to observe it in live meiocytes. As far as we know, there have been no attempts to study INM in live anthers on purpose; however, there were some cases when INM was documented in live *Arabidopsis* meiocytes accidentally (Varas *et al*., 2015; Yang *et al*., 2020, 2022).

Despite the advantages of all the aforementioned techniques, it seems that aldehyde fixation is the best way to investigate fine cellular structure of meiocyte columns. Unfortunately, aldehyde fixatives have a rather weak penetration ability, and anthers or at least spikes have to be dissected from plants prior to aldehyde fixation. These manipulations with unfixed tissues pose a risk of mechanical damage. Nevertheless, aldehyde fixation combined with volume microscopy enables us to perform observations unachievable by any other techniques. For light microscopy, this fixation gives a more detailed picture of studied cells with clear cytoplasm and prominent chromosome structure in the meiocyte, which helps to detect a significantly greater number of INM instances than in columns after alcohol fixation. For SBF-SEM, the treatment with aldehydes is critical, and only this type of fixation can be employed for sample preparation (Cocks *et al*., 2018; Courson *et al*., 2021).

Among vLM protocols, we chose CLSM and BFSM for the examination of the meiocytes after aldehyde fixation. Confocal laser scanning microscopy is used widely nowadays and needs no introduction. It allows 3-D imaging of structures of interest selectively stained by fluorescent dyes in rather big tissue fragments. Nonetheless, in some situations fluorescent dyes are unable to penetrate all the nuclei in a column and a substantial amount of the dye could be retained by the cytoplasm, thereby producing a strong fluorescent background preventing 3-D imaging. Another key point in the current work is the time of scanning of one sample. Scanning of a rye meiocyte column with sufficient quality by CLSM took hours. Because we intended to assess dozens of meiocyte columns to estimate the frequency of INM, it was quite challenging to perform CLSM for this purpose. In comparison, the scanning of one sample by BFSM takes less than 1 min. In this approach, serial optical sections of the routinely stained meiocyte columns were generated successfully. Acetocarmine was chosen because it penetrates cells fast and stains them quite intensely, helping to register more details of cell structure. Nevertheless, routine staining is not selective and requires that an investigator perform segmentation with artificial painting of nuclei to build a 3-D model such as the one in Fig. 2, which is quite a time-consuming and laborious procedure. Likely, there is no need to build 3-D models for every sample to determine INM frequency. The subsequent analysis of the images obtained by scanning allows examination of every cell and nucleus in a meiocyte column and detection of the majority of INM cases. Here we built 3-D models for a limited number of the scanned meiocyte columns for illustrative purposes. There is no doubt that state-of-the-art neural network protocols could solve the above-mentioned segmentation problems in future projects.

Thus, we chose routine staining combined with BFSM to assess the frequency of INM in rye meiocyte columns. This approach helped us to determine INM frequency in >100 meiocyte columns containing ~10 000 meiocytes. As a result, we can conclude that INM in rye male meiosis is a frequent and highly stage-specific process. At leptotene/zygotene it could be observed in almost every meiocyte. Owing to the large number of the examined cells, we were able to detect rare cases of INM at pachytene and diplotene/diakinesis stages and to conclude that there is no INM at later stages in the studied plants. This finding contradicts what we observed previously in tobacco by SBF-SEM, where a rather high rate of INM was registered throughout prophase I, and even later, at the anaphase I stage, INM had a frequency of ~20 % (Mursalimov *et al*., 2021). These data indicate that there are two types of plant species: plants where INM is strictly limited to certain stages and plants where it is present throughout meiosis. A hypothesis could be advanced that there is a difference in the occurrence pattern between monocots and dicots.

The frequency of INM in male meiocytes of the same rye line, as determined on squashed preparations, has been estimated as 2.5–12.65 % (Sidorchuk *et al*., 2016; Mursalimov *et al*., 2022). In comparison with the results of the current work, where ~77 % of meiocytes were involved in INM as estimated by BFSM, we can conclude that INM frequency has been underestimated in rye male meiosis by at least 6-fold. In other words, in the best scenario only every sixth instance of INM is detected in rye anthers by the common microscopic techniques widely used for determining INM frequency. A similar situation transpired when we evaluated INM frequency in tobacco male meiosis on squashed preparations and by SBF-SEM (Mursalimov *et al*., 2016, 2021): it was found that the INM frequency estimated on the squashed preparations is ~0.6 % versus ~95 % as determined by SBF-SEM, i.e. the common

approach can detect only one INM instance out of every 150 in tobacco meiosis. Extrapolation to other species is hard to resist: INM has been documented in hundreds of plant species, usually at low frequency, and in all these articles, only squashed preparations have been used for the INM frequency estimation (Negron-Ortiz, 2007; Reis *et al*., 2016; Khan *et al*., 2018; Kaur and Singhal, 2019; Tel-Zur *et al*., 2020). Consequently, we propose that INM frequency has been underestimated in the same manner in all these papers owing to the technical limitations.

One significant advantage of working with rye male meiosis is that meiocyte columns can be dissected from rye anthers rather easily. Previous attempts to study INM in dissected meiocyte columns of cereals have been performed in *Thinopyrum* sp. and its hybrids with wheat (Li *et al*., 2009) as well as in barley (Kravets, 2011, 2013). On the other hand, no volume microscopy techniques have been applied to the imaging of meiocyte columns in the above-mentioned articles, and only some INM cases have been suitable for observation. Thus, the dissection of meiocyte columns with preservation of their 3-D structure should be combined with volume microscopy imaging to detect the majority of INM cases. It should be mentioned that some NPs cannot be detected by any light microscopes owing to the small size of their NPs, which hides them from examination.

In turn, vEM has no limitations in terms of the size of the NPs that can be detected, and all the instances of INM are documented when this approach is selected. We are not aware of any studies involving vEM techniques other than SBF-SEM to image plant male meiocytes. By SBF-SEM, we analysed a smaller amount of material than by BFSM, eight meiocyte columns versus 115, but imaging at ultrastructural resolution was carried out this way. It allowed us to prove that the conclusions about INM frequency and dynamics drawn from BFSM are valid. After having counted every instance of INM, we can state that the INM frequency estimates do not differ much from those obtained by BFSM: 77 % according to BFSM versus 87 % according to SBF-SEM. Therefore, roughly 10 % of INM instances are hidden from observation during BFSM. Taking into account the time and effort required for SBF-SEM protocols, BFSM is a more suitable approach to the estimation of INM frequency in dozens and hundreds of meiocyte columns within a short period. We believe that the proposed approach to INM observation in meiocyte columns by vLM techniques may be adapted to different plant species, including non-cereal ones, and owing to its simplicity will help to estimate INM frequency in male meiosis of many species with sufficient accuracy.

SBF-SEM also proved the stage-specific nature of INM. There are no instances of INM before meiosis or at pachytene and later meiotic stages according to SBF-SEM. Nevertheless, because of its high resolution, not attainable by light microscopy, SBF-SEM enabled us to notice CCs connecting meiocytes at all the analysed stages. It is important to stress that CCs connect meiocytes at all the investigated stages, but INM happens in a strictly limited set of meiosis stages. These findings do not support the idea that INM is induced by processing of the plant material because the material was treated in the same way at all the examined stages. A difference in CC formation is noticeable between dicots and monocots. In rye meiocytes, CCs are situated uniformly across the cell surface except for the site in contact with tapetal cells, whereas in tobacco CCs form clusters in a few regions of the cell surface. Nevertheless, the ultrastructure of CCs in rye does not differ from that previously observed in tobacco meiocytes (Mursalimov *et al*., 2021). Another appreciable difference between dicots and monocots is the emergence of a special structure (via callose deposition) known as a callose spine in the central part of meiocyte columns (Bennett *et al*., 1973). In rye, these structures arise quite fast at the beginning of meiosis owing to unequal callose deposition around meiocytes, and this spine fills the central part of the meiocyte columns and then disappears rapidly, forming a central cavity. No structures like a callose spine were detected in tobacco meiosis despite the highly uneven callose deposition observed in this species as well (Mursalimov *et al*., 2021). The callose blocks some CCs in rye meiocytes, and it is possible that rapid stage-specific transformation of the callose wall at the beginning of meiotic prophase I could be connected to the stage-specific activation of INM in rye meiosis at this time point. This question deserves additional research, and the techniques suggested in the present work may be helpful because such structures as a callose spine cannot be studied by common techniques such as squashed preparations.

It was previously stated that in monocots INM could be detected between tapetal cells and meiocytes (Silkova *et al*., 2021). The current work does not support these observations. We did not find a single case of INM between tapetal cells and meiocytes at any stages; furthermore, no CCs were found between these two types of cells. Considering that in tobacco anthers subjected to SBF-SEM no cases of INM and no CC formation between tapetal cells and meiocytes were detected either (Mursalimov *et al*., 2021), the finding of INM between tapetal cells and meiocytes by light microscopy in any species should be viewed with scepticism.

SBF-SEM confirmed the result obtained after the examination of INM by vLM, namely, that the migrating part of a nucleus never separates from the source nucleus even after entering a neighbouring cell. No instances of micronucleus formation were found in the studied cells at any stage. A thorough examination of a series of ultrastructural images did not reveal a single case of NP disruption. The same observation was made when tobacco meiocytes were researched by SBF-SEM (Mursalimov *et al*., 2021). The migrating part of a nucleus never separates from the source nucleus during INM in plant meiocytes. Thus, the generally accepted point of view that the main outcome of INM is micronucleus formation (Barton *et al*., 2014; Reis *et al*., 2016) should be rejected. It seems that all the previously published cases of micronucleus observation in plant meiocytes after INM are a result of artificial separation of NPs from their nucleus during sample preparation or misinterpretation during examination of individual tissue sections.

Interpreting the data acquired by SBF-SEM, we also noticed that, usually during INM, meiocyte nuclei retain their position in the central part of the cell, i.e. they do not migrate as the whole structure but rather form migrating NPs, which can be quite long in some cases and even be comparable in length to a nucleus diameter. In tobacco, no cases of formation of such extended NPs have been observed; moreover, in tobacco meiosis there are rather frequent instances of a whole nucleus migrating into a neighbouring cell, giving rise to binucleated and enucleated meiocytes (Mursalimov *et al*., 2021, 2022*a*).

It is worth emphasizing that NPs could be seen at the premeiotic stage when no cases of INM are detectable. At this stage, they do not reach the status of CCs, and only at leptotene do they cross the cell wall and enter a neighbouring cell. NPs that do not penetrate the cell wall are also observed at zygotene, the last stage where INM is seen. It seems that initially, at the premeiotic stage, NPs are too short to enter another cell; next, at leptotene, they extend and cross the cell wall with unknown consequences, and then at zygotene they start to return to their source cell. In other words, we do not believe that this is a combination of random events; rather, this is a process that has its own dynamics. Further research is needed to investigate the consequences of this phenomenon.

Some damaged cells seen in every sample scanned by SBF-SEM should be discussed separately. It is difficult to determine whether these cells were damaged owing to some endogenous factors before the experiments or because of an external factor applied during sample preparation. It is possible that both types of factors contributed to the observed cell damage. Regardless of the origin of these damaged cells, as already mentioned, they were detected in all the samples, including the premeiotic stage, where not a single instance of INM was registered. Such damaged cells were absent in tobacco meiocytes studied by SBF-SEM, although most of meiocytes were involved in INM (Mursalimov *et al.*, 2021). Thus, there is no obvious correlation between the presence of damaged cells and INM in rye and tobacco meiosis. Taking into account the cryofixation experiments performed on meiocytes of both of these species, we think that it is highly unlikely that the cell damage is the reason for INM. Nevertheless, we can theorize that the manifestation of INM could be substantially modified during sample preparation. If cells are damaged during INM, then migrating nuclei undergo damage as well, and if the nuclei are destroyed, then they leave structureless chromatin like the chromatin that we observed in some cases after aldehyde fixation in rye meiocyte columns. It seems that mechanical impact plays a key role in such damage and should be avoided at all costs.

Thus, INM was constantly observed in rye meiocytes at certain stages of male meiosis in all the examined samples, no matter which techniques of fixation and imaging were applied. The volume microscopy methods indicate that the real frequency of INM in rye meiosis is sufficiently higher than estimated on widely used squashed preparations and tissue sections, and that most rye male meiocytes participate in INM. Similar patterns of INM were previously observed in male meiosis of a taxonomically distant species, tobacco, when its meiocytes were imaged by vEM. Even though male meiosis of only these two species has been analysed by vEM, there are hundreds of other plant species where INM has been documented on squashed preparations (He *et al.*, 2004; Pécrix *et al.*, 2011; Mursalimov *et al.*, 2013; Páez *et al.*, 2021). The high prevalence and constant presence of INM during meiosis of rye and tobacco allows us to conclude that INM is either a programmed process, i.e. a normal part of male meiosis of many (or even all) plant species, or a tricky artefact that cannot be avoided in any experiments involving manipulations of plant anthers. Anyway, INM appears to be an obligatory phenomenon for plant male meiosis and should not be ignored.

If we assume that INM is a consequence of some form of artificial factor, then we have to admit that there is no protocol that can prevent it, and even cryofixation of whole organs cannot help. As an unavoidable process, it is important in all studies on plant male meiosis and in breeding and crop improvement programmes. Aside from the influence of INM on laboratory and agricultural plants, questions arise about wild-type plant populations. If meiocyte nuclei start migrating because of the slightest impact that we even cannot account for, then how do plants manage to avoid this stressor in their natural environment, where they are constantly exposed to biotic and abiotic factors? How do plants somehow manage to form fertile pollen if their male meiocytes can be influenced so easily, and in this regard, what potential contribution can INM make to plant fertility in the wild? If INM is not a programmed natural process, then it is essential to determine what exactly induces such behaviour of nuclei. Why are meiocyte nuclei so mobile only at a certain stage of rye meiosis? Could this specific feature be connected to peculiarities of the organization of their cytoskeleton or the functioning of CCs? Is it possible for meiocytes to get back on the track of normal meiotic division if INM is a consequence of an artificial factor? Is it possible to manipulate this migration? Addressing these questions can substantially elucidate many aspects of plant cell biology and developmental biology.

In light of the available evidence from both the literature and our own work, we tend to consider INM a natural process of male meiosis in at least two plant species, tobacco and rye. Many researchers have been regarding INM in plant meiosis as a natural phenomenon involved either in unreduced-pollen production (Farooq *et al.*, 2014; Fakhri *et al.*, 2016; Djafri-Bouallag *et al.*, 2019; Tel-Zur *et al.*, 2020) or in a response to stress (Kalinka *et al.*, 2010; Kravets, 2011; Kravets *et al.*, 2022). By contrast, INM has never been considered a constant part of plant male meiosis. This new status of INM requires reconsideration of its role in plant meiosis. On the one hand, the detection of INM in all the studied samples of rye grown under normal conditions in a greenhouse at certain meiotic stages makes it unlikely that INM is a part any kind of stress response. On the other hand, we did not find cases of binucleated meiocytes resulting from INM in rye meiosis; such cases in tobacco were demonstrated previously (Mursalimov and Deineko, 2011). Nonetheless, there were documented cases of direct contacts between NPs and nuclei of neighbouring cells in the current work; therefore, their potential fusion leading to the formation of aneuploid or unreduced pollen cannot be fully ruled out.

It should be noted that the NPs in plant meiocytes remarkably resemble unusual nuclear structures observed in the placental tissue of the carnivorous plant *Utricularia nelumbifolia*. The cell nuclei in this case also form extended NPs, named chromatubules (chromatin-filled tubules), which enter neighbouring cells and make contact with other nuclei (Płachno *et al.*, 2017). Nonetheless, in comparison with INM in plant meiocytes, the formation of chromatubules is a unique phenomenon described only in one species of carnivorous plants and undetectable in closely related species. Another intriguing observation reported about these chromatubules is that they contain cytoskeleton-like structures inside. Nothing of this kind can be observed in NPs during INM in plant meiocytes, where the cytoskeleton attaches to the external side of the nuclear membrane (Sidorchuk *et al.*, 2016; Mursalimov and Deineko, 2018). A possible reason is that chromatubules in the placental

tissue of *U. nelumbifolia* seem to be rather stable structures whereas NPs in plant meiocytes exist only for a short period. Unfortunately, there is still not enough data to determine the functions of chromatubules, and there is no published information about INM in the meiosis of *U. nelumbifolia*. Nevertheless, it is important to stress that it was 3-D ultrastructural analysis that played a key role in the detection of the aforementioned unusual nuclear structures (Płachno *et al.*, 2017).

Thus, the reasons for INM in plant meiosis are still debatable, but the current work was not aimed at addressing this issue, and further studies are needed to investigate the causes and consequences of INM. The key point of the current work is the obligatory nature of this phenomenon, regardless of its origin. First and foremost, the scientific community working in the field of sexual pant reproduction has to admit it at least for rye and tobacco. Second, we need to transition away from perceiving the structure of meiocytes in 2-D and discontinue the use of squashed preparations for INM investigation. New protocols for INM study should preserve intact structure not only of individual meiocytes but also of whole meiocyte columns, and imaging should be performed by volume microscopy techniques with sufficient magnification/resolution that allows detection of all the NPs, including the smallest ones.

In this context, it must be pointed out that many researchers may be unable to detect INM in their samples, even when nuclear migration is prominent and perfectly amenable to analysis. This problem could be due to their lack of familiarity with the INM phenomenon, leading them to overlook it simply because they are not aware that nuclear migration between meiocytes is possible. In the present work, we (having sufficient experience with examination of INM in rye and other species) purposely searched for INM in rye meiocytes. Even in this study, we could not detect many instances of INM until 3-D reconstruction of the images. Artificial intelligence trained to detect INM cases in images may simplify the detection and analysis of this phenomenon in plant male meiosis.

Taking into account the rapid development of techniques of volume microscopy and of image data analysis, we believe that limitations of conventional protocols of plant male meiosis analysis are responsible for the considerable underestimation of the frequency and importance of INM and will be overcome soon. Although the focus of the present paper is on INM, it seems that 3-D analysis of meiocyte columns instead of the 2-D analysis of meiocytes has good potential to reveal many other interesting aspects of plant meiosis still hiding from researchers behind technical limitations and the inadequacy of 2-D perception of complex cell structures.

SUPPLEMENTARY DATA

Supplementary data are available at *Annals of Botany* online and consist of the following. Figure S1: rye meiocyte columns imaged by vLM. Figure S2: CCs in the cell wall of rye meiocytes. (A–D) CCs indicated by arrows in the individual ultrastructural images. (E–H) 3-D reconstructions of the location of CCs in rye meiocytes. Yellow colour denotes CCs and purple denotes plasmodesmata. (A, E) Premeiotic stage, (B, F) leptotene, (C, G) zygotene, (D, H) pachytene. Scale bars = 2 µm in A–D and 5 µm in E–H. Video S1: 3-D reconstructions of the meiocyte column at the premeiotic stage imaged by BFSM; the same sample as in Fig. 2B, C. Video S2: 3-D reconstructions of the meiocyte column at leptotene/zygotene imaged by BFSM; the same sample as in Fig. 2D. Video S3: 3-D reconstructions of a meiocyte column at leptotene/zygotene imaged by BFSM; the same sample as in Fig. 2E, F. Video S4: 3-D reconstructions of a meiocyte column at pachytene imaged by BFSM; the same sample as in Fig. 2H, I. Video S5: 3-D reconstructions of a meiocyte column at the premeiotic stage imaged by SBF-SEM; the same sample as in Fig. 3A–D. Video S6: 3-D reconstructions of a meiocyte column at the leptotene stage imaged by SBF-SEM; the same sample as in Fig. 3E–H. Video S7: 3-D reconstructions of the meiocyte column at the zygotene stage imaged by SBF-SEM; the same sample as in Fig. 3I–L. Video S8: 3-D reconstructions of a meiocyte column at the pachytene stage imaged by SBF-SEM; the same sample as in Fig. 3M–P.

DATA AVAILABILITY

The data presented in the article and Supplementary Data should be enough for reproducing our results; raw data are available from the corresponding author upon request.

CONFLICT OF INTEREST

The authors declare no competing interests.

FUNDING

The reported study was funded by the Russian Foundation for Basic Research and by the Japan Society for Promotion of Science within research projects No. 21-54-50001 and JPJSBP120214813. The light microscopy performed at the Multi-Access Center for Microscopy of Biological Objects was supported by the Institute of Cytology and Genetics' project No. FWNR-2022-0015. The use of the Electron Microscopy Unit at the National Institute for Physiological Sciences was supported by the Joint Research Program (22NIPS208) of the National Institute for Physiological Sciences.

ACKNOWLEDGEMENTS

We thank Atsuko Imai, Nobuko Hattori (National Institute for Physiological Sciences), Harumi Watanabe and Kimiyo Yagai (Jichi Medical University) for their technical assistance.

REFERENCES

Ahn YJ, **Cuacos M**, **Ayoub MA**, **Kappermann J**, **Houben A**, **Heckmann S. 2020**. In planta delivery of chemical compounds into barley meiocytes: EdU as compound example In: *Methods in molecular biology*.

Arnoldy W. 1900. Beitrage zur Morphologie der Gymnospermen. IV. Was sind die «Keimblaschen» oder «Hofmeisters-Korperchen» in der Eizelle der Arbietineen. *Flora* **87**: 194–204.

Barton DA, **Cantrill LC**, **Law AMK**, **Phillips CG**, **Sutton BG**, **Overall RL. 2014**. Chilling to zero degrees disrupts pollen formation but not meiotic

microtubule arrays in *Triticum aestivum* L. *Plant, Cell & Environment* **37**: 2781–2794. doi:10.1111/pce.12358.

Baskin TI, **Miller DD**, **Vos JW**, **Wilson JE**, **Hepler PK. 1996**. Cryofixing single cells and multicellular specimens enhances structure and immunocytochemistry for light microscopy. *Journal of Microscopy* **182**: 149–161. doi:10.1046/j.1365-2818.1996.135417.x.

Belevich I, **Joensuu M**, **Kumar D**, **Vihinen H**, **Jokitalo E. 2016**. Microscopy Image Browser: a platform for segmentation and analysis of multidimensional datasets. *PLoS Biology* **14**: e1002340. doi:10.1371/journal.pbio.1002340.

Bennett MD, **Rao MK**, **Smith JB**, **Bayliss MW. 1973**. Cell development in the anther, the ovule, and the young seed of *Triticum aestivum* L. var. Chinese Spring. *Philosophical Transactions of the Royal Society of London B Biological Sciences* **266**: 39–81.

Bennici S, **Distefano G**, **Las Casas G**, ***et al***. **2019**. Temperature stress interferes with male reproductive system development in clementine (*Citrus clementina* Hort. ex. Tan.). *Annals of Applied Biology* **175**: 29–41. doi:10.1111/aab.12508.

Cocks E, **Taggart M**, **Rind FC**, **White K. 2018**. A guide to analysis and reconstruction of serial block face scanning electron microscopy data. *Journal of Microscopy* **270**: 217–234. doi:10.1111/jmi.12676.

Courson JA, **Landry PT**, **Do T**, ***et al***. **2021**. Serial block-face scanning electron microscopy (SBF-SEM) of biological tissue samples. *Journal of Visualized Experiments* **2021**: 10.3791/62045.

Djafri-Bouallag L, **Ourari M**, **Sahnoune M. 2019**. A cytogenetic and pollen study of annual *Medicago* species from Soummam Valley (Northeastern of Algeria). *Acta Botanica Croatica* **78**: 82–90. doi:10.2478/botcro-2019-0010.

Dukowic-Schulze S, **van der Linde K. 2021**. Oxygen, secreted proteins and small RNAs: mobile elements that govern anther development. *Plant Reproduction* **34**: 1–19. doi:10.1007/s00497-020-00401-0.

Fadón E, **Herrero M**, **Rodrigo J. 2019**. Anther and pollen development in sweet cherry (*Prunus avium* L.) in relation to winter dormancy. *Protoplasma* **256**: 733–744. doi:10.1007/s00709-018-01332-4.

Fakhri Z, **Mirzaghaderi G**, **Ahmadian S**, **Mason AS. 2016**. Unreduced gamete formation in wheat × *Aegilops* spp. hybrids is genotype specific and prevented by shared homologous subgenomes. *Plant Cell Reports* **35**: 1143–1154. doi:10.1007/s00299-016-1951-9.

Farooq U, **Lovleen**, **Saggoo MIS**. **2014**. Male meiosis and behaviour of sex chromosomes in different populations of *Rumex acetosa* L. from the Western Himalayas, India. *Plant Systematics and Evolution* **300**: 287–294.

Feijo JA, **Pais MS. 1989**. Cytomixis in meiosis during the microsporogenesis of *Ophrys lutea*: an ultrastructural study. *Caryologia* **42**: 37–48.

Gates RR. 1908. A study of reduction in *Oenothera rubrinervis*. *Botanical Gazette* **46**: 1–34. doi:10.1086/329610.

Gates RR. 1911. Pollen formation in *Oenothera gigas*. *Annals of Botany* **os-25**: 909–940. doi:10.1093/oxfordjournals.aob.a089373.

Giorgetti L, **Martini G**, **Geri C**, **Ronchi VN**, **Castiglione MR. 2007**. Methylated DNA sequence extrusion during plant early meiotic prophase. *Caryologia* **60**: 279–289.

Harwood R, **Goodman E**, **Gudmundsdottir M**, ***et al***. **2020**. Cell and chloroplast anatomical features are poorly estimated from 2D cross-sections. *New Phytologist* **225**: 2567–2578. doi:10.1111/nph.16219.

He Z, **Wang H**, **Li J**, **Ye Q**, **Taylor WC. 2004**. Chromosome behavior during meiosis and development of spore mother cells in the Chinese quillwort *Isoetes sinensis* T. C. Palmer (Isoetaceae). *American Fern Journal* **94**: 183–195. doi:10.1640/0002-8444(2004)094[0183:cbdmad]2.0.co;2.

Heslop-Harrison J. 1966. Cytoplasm connections between angiosperm meiocytes. *Annals of Botany* **30**: 221–222. doi:10.1093/oxfordjournals.aob.a084069.

Kalinka A, **Achrem M**, **Rogalska SM. 2010**. Cytomixis-like chromosomes/chromatin elimination from pollen mother cells (PMCs) in wheat-rye allopolyploids. *Nucleus* **53**: 69–83. doi:10.1007/s13237-010-0002-0.

Kaur D, **Singhal VK. 2019**. Meiotic abnormalities affect genetic constitution and pollen viability in dicots from Indian cold deserts. *BMC Plant Biology* **19**: 10.

Khan NA, **Singhal VK**, **Gupta RC. 2018**. First record of chromosome count and cytomixis in an endemic species of *Clematis ladakhiana* Grey-Wilson (Ranunculaceae) from cold deserts of Jammu and Kashmir. *Caryologia* **71**: 233–237. doi:10.1080/00087114.2018.1460520.

Koernicke M. 1901. Über Ortsveränderung von Zellkernen. *SB Der Niederrheinischen Gesellschaft Fur Natur- Und Heilkunde. Bonn*: 14–25.

Kolczyk J, **Tuleja M**, **Płachno BJ. 2015**. Histological and cytological analysis of microsporogenesis and microgametogenesis of the invasive species *Galinsoga quadriradiat*a Ruiz & Pav. (Asteraceae). *Acta Biologica Cracoviensia Series Botanica* **57**: 89–97.

Kravets E. 2011. The role of cell selection for pollen grain fertility after treatment of barley sprouts (*Hordeum distichum* L.) with UV-B irradiation. *Acta Biologica Slovenica* **54**: 31–41.

Kravets E. 2013. Cytomixis and its role in the regulation of plant fertility. *Russian Journal of Developmental Biology* **44**: 113–128.

Kravets EA, **Plokhovska SG**, **Yemets AI**, **Blume YB. 2022**. UV-B stress and plant sexual reproduction. In: **Kataria S**, **Singh VP**. eds. *UV-B radiation and crop growth. Plant life and environment dynamics*. Singapore: Springer, 293–318. doi:10.1007/978-981-19-3620-3_14.

Kumar S, **Jeelani SM**, **Rani S**, **Gupta RC**, **Kumari S. 2013**. Cytology of five species of subfamily Papaveroideae from the Western Himalayas. *Protoplasma* **250**: 307–316. doi:10.1007/s00709-012-0413-7.

Li B, **Xu F. 2019**. Formation pattern in five types of pollen tetrad in *Pseuduvaria trimera* (Annonaceae). *Protoplasma* **256**: 53–68. doi:10.1007/s00709-018-1282-5.

Li XF, **Song ZQ**, **Feng DS**, **Wang HG. 2009**. Cytomixis in *Thinopyrum intermedium*, *Thinopyrum ponticum* and its hybrids with wheat. *Cereal Research Communications* **37**: 353–361. doi:10.1556/crc.37.2009.3.4.

Li J, **Farmer AD**, **Lindquist IE**, ***et al***. **2012**. Characterization of a set of novel meiotically-active promoters in *Arabidopsis*. *BMC Plant Biology* **12**: 104.

Liao J, **Zhang J**, **Wei X**, ***et al***. **2020**. Cytological abnormalities during pollen development in interspecific hybrids of *Nicotiana*. *Crop and Pasture Science* **71**: 1029–1040. doi:10.1071/cp20155.

Munro KC, **Jackson JRM**, **Hartling I**, **Sumner MJ**, **Friedman CMR. 2014**. Anther and pollen development in the lodgepole pine dwarf mistletoe (*Arceuthobium americanum*) staminate flower. *Botany* **92**: 203–214.

Mursalimov SR, **Deineko EV. 2011**. An ultrastructural study of cytomixis in tobacco pollen mother cells. *Protoplasma* **248**: 717–724. doi:10.1007/s00709-010-0234-5.

Mursalimov S, **Deineko E. 2018**. Cytomixis in plants: facts and doubts. *Protoplasma* **255**: 719–731. doi:10.1007/s00709-017-1188-7.

Mursalimov SR, **Sidorchuk YV**, **Deineko EV. 2013**. New insights into cytomixis: specific cellular features and prevalence in higher plants. *Planta* **238**: 415–423. doi:10.1007/s00425-013-1914-0.

Mursalimov S, **Sidorchuk Y**, **Demidov D**, **Meister A**, **Deineko E. 2016**. A rise of ploidy level influences the rate of cytomixis in tobacco male meiosis. *Protoplasma* **253**: 1583–1588. doi:10.1007/s00709-015-0907-1.

Mursalimov S, **Ohno N**, **Matsumoto M**, **Bayborodin S**, **Deineko E. 2021**. Serial block-face scanning electron microscopy reveals that intercellular nuclear migration occurs in most normal tobacco male meiocytes. *Frontiers in Plant Science* **12**: 672642. doi:10.3389/fpls.2021.672642.

Mursalimov S, **Ohno N**, **Deineko E. 2022***a*. Intercellular nuclear migration in cryofixed tobacco male meiocytes. *Protoplasma* **259**: 1371–1376. doi:10.1007/s00709-021-01725-y.

Mursalimov S, **Permyakova N**, **Deineko E**, **Silkova O. 2022***b*. Cytomixis in wheat male meiosis: influence analysis of the substitution of chromosome 1A, 2D, 5A, or 5D. *Botany Letters* **169**: 327–336. doi:10.1080/23818107.2022.2074889.

Negron-Ortiz V. 2007. Chromosome numbers, nuclear DNA content, and polyploidy in *Consolea* (Cactaceae), an endemic cactus of the Caribbean Islands. *American Journal of Botany* **94**: 1360–1370. doi:10.3732/ajb.94.8.1360.

Ohno S, **Terada N**, **Ohno N**, **Saitoh S**, **Saitoh Y**, **Fujii Y. 2010**. Significance of 'in vivo cryotechnique' for morphofunctional analyses of living animal organs. *Journal of Electron Microscopy* **59**: 395–408. doi:10.1093/jmicro/dfq058.

Ohno N, **Terada N**, **Bai Y**, ***et al***. **2008**. Application of cryobiopsy to morphological and immunohistochemical analyses of xenografted human lung cancer tissues and functional blood vessels. *Cancer* **113**: 1068–1079. doi:10.1002/cncr.23701.

Ono K, **Gotoh H**, **Nomura T**, ***et al***. **2022**. Ultrastructural characteristics of oligodendrocyte precursor cells in the early postnatal mouse optic nerve observed by serial block-face scanning electron microscopy. *PLoS One* **17**: e0278118. doi:10.1371/journal.pone.0278118.

Páez V de los A, **Andrada AR**, **Kumar P**, **Caro MS. 2021**. Cytomixis in angiosperms from Northwestern Argentina. *Botany Letters* **168**: 536–545.

Pécrix Y, **Rallo G**, **Folzer H**, **Cigna M**, **Gudin S**, **Le Bris M. 2011**. Polyploidization mechanisms: temperature environment can induce diploid gamete formation in *Rosa* sp. *Journal of Experimental Botany* **62**: 3587–3597. doi:10.1093/jxb/err052.

Płachno BJ, **Świątek P**, **Jobson RW**, **Małota K**, **Brutkowski W. 2017**. Serial block face SEM visualization of unusual plant nuclear tubular extensions in a carnivorous plant (*Utricularia*, Lentibulariaceae). *Annals of Botany* **120**: 673–680. doi:10.1093/aob/mcx042.

Reis A, **Sousa SM**, **Viccini L. 2016**. High frequency of cytomixis observed at zygotene in tetraploid *Lippia alba*. *Plant Systematics and Evolution* **302**: 121–127.

Reis AC, **Chester M**, **de Sousa SM**, ***et al***. **2022**. Chromosomal view of *Lippia alba*, a tropical polyploid complex under genome stabilization process. *Protoplasma* **259**: 33–46. doi:10.1007/s00709-021-01636-y.

Rensing KH, **Samuels AL**, **Savidge RA. 2002**. Ultrastructure of vascular cambial cell cytokinesis in pine seedlings preserved by cryofixation and substitution. *Protoplasma* **220**: 39–49. doi:10.1007/s00709-002-0033-8.

Schindelin J, **Arganda-Carreras I**, **Frise E**, ***et al***. **2012**. Fiji: an open-source platform for biological-image analysis. *Nature Methods* **9**: 676–682. doi:10.1038/nmeth.2019.

Senft SL, **Argiro VJ**, **VanZandt WL. 1990**. Volume microscopy of biological specimens based on non-confocal imaging techniques. In: Proceedings of the First IEEE Conference on Visualization: Visualization `90, San Francisco, CA, USA: IEEE, 424–428. doi:10.1109/VISUAL.1990.146413.

Sheehan MJ, **Pawlowski WP. 2009**. Live imaging of rapid chromosome movements in meiotic prophase I in maize. *Proceedings of the National Academy of Sciences of the USA* **106**: 20989–20994. doi:10.1073/pnas.0906498106.

Shunmugam ASK, **Bollina V**, **Dukowic-Schulze S**, ***et al***. **2018**. MeioCapture: an efficient method for staging and isolation of meiocytes in the prophase I sub-stages of meiosis in wheat. *BMC Plant Biology* **18**: 293. doi:10.1186/s12870-018-1514-z.

Sidorchuk YV, **Novikovskaya AA**, **Deineko EV. 2016**. Cytomixis in the cereal (Gramineae) microsporogenesis. *Protoplasma* **253**: 291–298. doi:10.1007/s00709-015-0807-4.

Silkova OG, **Ivanova YN**, **Loginova DB**, **Solovey LA**, **Sycheva EA**, **Dubovets NI. 2021**. Karyotype reorganization in wheat–rye hybrids obtained via unreduced gametes: is there a limit to the chromosome number in triticale? *Plants* **10**: 2052. doi:10.3390/plants10102052.

Somashekar H, **Mimura M**, **Tsuda K**, **Nonomura KI. 2023**. Rice GLUCAN SYNTHASE-LIKE5 promotes anther callose deposition to maintain meiosis initiation and progression. *Plant Physiology* **191**: 400–413. doi:10.1093/plphys/kiac488.

Stronghill PE, **Azimi W**, **Hasenkampf CA. 2014**. A novel method to follow meiotic progression in *Arabidopsis* using confocal microscopy and 5-ethynyl-2′-deoxyuridine labeling. *Plant Methods* **10**: 33. doi:10.1186/1746-4811-10-33.

Studer D, **Humbel BM**, **Chiquet M. 2008**. Electron microscopy of high pressure frozen samples: bridging the gap between cellular ultrastructure and atomic resolution. *Histochemistry and Cell Biology* **130**: 877–889. doi:10.1007/s00418-008-0500-1.

Tel-Zur N, **Mouyal J**, **Zurgil U**, **Mizrahi Y. 2020**. In support of Winge's theory of 'Hybridization followed by chromosome doubling'. *Frontiers in Plant Science* **11**: 954.

Urakubo H, **Bullmann T**, **Kubota Y**, **Oba S**, **Ishii S. 2019**. UNI-EM: an environment for deep neural network-based automated segmentation of neuronal electron microscopic images. *Scientific Reports* **9**: 19413. doi:10.1038/s41598-019-55431-0.

Varas J, **Graumann K**, **Osman K**, ***et al***. **2015**. Absence of SUN1 and SUN2 proteins in *Arabidopsis thaliana* leads to a delay in meiotic progression and defects in synapsis and recombination. *Plant Journal* **81**: 329–346. doi:10.1111/tpj.12730.

Yang C, **Hu B**, **Portheine SM**, **Chuenban P**, **Schnittger A. 2020**. State changes of the HORMA protein ASY1 are mediated by an interplay between its closure motif and PCH2. *Nucleic Acids Research* **48**: 11521–11535. doi:10.1093/nar/gkaa527.

Yang C, **Sofroni K**, **Hamamura Y**, ***et al***. **2022**. ZYP1-mediated recruitment of PCH2 to the synaptonemal complex remodels the chromosome axis leading to crossover restriction. *Nucleic Acids Research* **50**: 12924–12937. doi:10.1093/nar/gkac1160.